Three operation regimes with an L-band ultrafast fiber laser passively mode-locked by graphene oxide saturable absorber

Junqing Zhao,[1] Yonggang Wang,[2] Shuangchen Ruan,[1,*] Peiguang Yan,[1] Han Zhang,[3] Yuen H. Tsang,[4] Jinhui Yang,[1] and Guoxi Huang[1]

[1]*Shenzhen Key Laboratory of Laser Engineering, Key Laboratory of Advanced Optical Precision Manufacturing Technology of Guangdong Higher Education Institutes, Shenzhen University, Shenzhen, Guangdong 518060, China*
[2]*State Key Laboratory of Transient Optics and Photonics, Xi'an Institute of Optics and Precision Mechanics, Chinese Academy of Sciences, Xi'an 710119, China*
[3]*College of Optoelectronic Engineering, Shenzhen University, ShenZhen 518060, China*
[4]*Department of Applied Physics, Hong Kong Polytechnic University, Hong Kong, China*
**Corresponding author: scruan@szu.edu.cn*

Received December 9, 2013; revised January 28, 2014; accepted January 28, 2014; posted January 29, 2014 (Doc. ID 202620); published March 6, 2014

We present three operation regimes with an L-band erbium-doped fiber laser passively mode-locked by a graphene oxide saturable absorber (GOSA) that is fabricated by using a wet chemical method. One is a stable state of single soliton emission with pulse duration of 426 fs, which is the shortest pulse duration ever achieved with an L-band design by employing GOSA as the mode-locker. The other two operation regimes include bound-state soliton and dual-wavelength nanosecond pulse generation, which are demonstrated for the first time by using the GOSA mode-locker. Our results further indicate the practical potential of GOSA in ultrafast fiber lasers for achieving various mode-locking regimes.

OCIS codes: (140.4050) Mode-locked lasers; (160.4236) Nanomaterials; (140.3510) Lasers, fiber.
http://dx.doi.org/10.1364/JOSAB.31.000716

1. INTRODUCTION

Passive mode-locking is a typical technique for ultrashort pulse generation, and a saturable absorber (SA) is a key element that starts the mode-locked operation of a laser resonator. Various SAs based on different materials have emerged over the past decades, such as dyes, ion-doped crystals and glasses, semiconductor SA mirrors (SESAMs), metal nanoparticals, carbon nanotubes (CNTs), graphene, graphene oxide (GO), and other topological insulators. Currently, SESAMs have been utilized for commercial ultrafast lasers, and their excellent performance over other traditional SAs is realized by well-developed semiconductor technologies in the electronics industry [1]. However, the fabrication of SESAMs needs expensive and high-precision clean-room-based equipment assisted with complex and specialized techniques. Besides that, SESAMs typically can only respond to the incident light within narrow wavelength bands (typically no more than 100 nm), and their response times are typically longer than 5 ps [2].

CNT-based devices have been regarded as promising SAs that can function better than SESAMs for their faster response (response time <1 ps), higher optical damage threshold, and low cost. Employing CNTs for starting the mode-locked operation of fiber lasers was first realized by Set and co-workers [2,3]. From then on, various CNT-based lasers have been reported, especially ultrafast all-fiber lasers due to their advantages over other bulk solid-state lasers including compact structure, high-quality optical beams and pulses, and adjust-free configuration. CNT-based fiber lasers have achieved significant progress. The shortest pulses from a fiber resonator using a CNT mode-locker can reach less than 100 fs through careful dispersion management [4–6]. Up to 5 GHz pulse repetition rates have been demonstrated by Yamashita *et al.* early in 2005 [7]. 1.5 nJ pulses with dechirped pulse duration of 250 fs can be generated from an all-normal dispersion ytterbium-doped fiber laser system by using an inline SA that is based on a fiber taper embedded in a composite of single-walled CNTs in a polymer host [8]. Some applications based on CNT-mode-locked fiber lasers have also been demonstrated. Zhang *et al.* demonstrated the mid-infrared Raman-soliton continuum generation by using a CNT mode-locked thulium-doped fiber laser as the pump source [9].

Although the reported results indicate that CNTs have shown good performance in ultrafast laser systems and can be highly promising SAs, it has been demonstrated that graphene exhibits many other merits compared with CNTs. The response wavelengths of CNTs are typically determined by their tube-diameter distribution. Thus, although CNT-based SAs have shown much wider saturable absorption bandwidths compared with SESAMs, their functional bandwidths are typically limited. The factors of CNTs including unavoidable bundles, catalysts, and attached amorphous carbons can induce large nonsaturable loss to CNT-based SAs [10], which is another drawback of CNTs. Graphene can effectively overcome these drawbacks of CNTs due to its unique two-dimensional atomic layer structure [10,11]. The most outstanding feature

of graphene is its wavelength-independent optical absorption property due to the linear dispersion of the Dirac electrons [1,10,11]. The saturable absorption mechanism of graphene has been proved to be Pauli blocking [10]. Graphene has also shown much faster responses, down to less than 100 fs, which is associated with carrier–carrier intraband collisions [12] and photo-excitation [10]. Graphene-based SAs (GSAs) used for passive mode-locking have been a hot topic since the first GSA mode-locked fiber laser was demonstated by Bao *et al.* [10]. Sub-200 fs pulses have been achieved by using GSA in a fiber laser [13]. Similar to CNTs, GSAs can also achieve ultrahigh repetition rate operation [14]. Using few-layered graphene as an SA, hundreds of experimental results have been demonstrated; the operational wavelengths have extended from around 800 nm [15] to more than 3 μm [16]. Significantly different from CNTs, which typically need to select certain tube-diameter distributions for different operational wavelength applications, GSAs can be used at various wavelengths without any change of the graphene. Thus, graphene can be another, more promising SA material.

Although few-layered GO was originally regarded as a precursor for graphene, it has also been verified to show as excellent a saturable absorption property as graphene [17,18]. Moreover, GO can be easily dissolved in water due to its hydrophilic nature associated with the oxygen functionalities [19]. This water-soluble property offers many more choices in preparing it for various applications. To make a SA device based on GO, different kinds of hosts or substrates had been demonstrated, such as polymer [20], solution [21], Si/SiO_2 [18], indium tin oxide [22], hydrophilic quartz [23,24], broadband reflective mirror [19,25], tapered fiber [26], and D-shaped fiber [27].

Using a GO SA (GOSA) for mode-locking was firstly realized by Bonaccorso *et al.* [28], where they reported a mode-locked laser delivering pulses with a duration of ~743 fs. The following GO-based mode-locking was realized in an all-fiber format by filling the few-layered GO solution into a hollow-core photonic crystal fiber [21]. Xu *et al.* proposed dissipative soliton generation in an erbium-doped fiber (EDF) laser with net normal dispersion [25]. Due to the highly chirped nature of dissipative solitons, the directly generated pulses were as long as 11 ps, which could be compressed from 11 ps to 542 fs by dechirping. Sobon also employed GOSA to realize the soliton mode-locking of an EDF laser with 3 dB bandwidth of ~9.3 nm [18]. Besides the 1.5 μm band fiber lasers, 2 μm band mode-locked lasers were also realized by using GOSA. Liu *et al.* demonstrated a GO mode-locked all-solid $Tm:YAlO_3$ laser operating at 2023 nm [24]. Jung *et al.* demonstrated a GO mode-locked thulium-doped fiber laser with soliton generation at 1.91 μm [27], where the GOSA was fabricated by spraying GO onto a D-shaped fiber, and the realization was based on evanescent field interaction.

Most of the mode-locked EDF lasers are designed for emission at the C-band. However, L-band ultrafast fiber lasers can also find wide applications, such as in frequency-doubled biomedical diagnostics [29,30]. Up to now, all the generated pulses from GO mode-locked EDF lasers are either conventional solitons [18,19,27] or dissipative solitons [25], mainly in the C-band.

In this paper, we demonstrate three operation regimes in a GO mode-locked fiber laser, including stable single-soliton operation, bound-state soliton generation, and dual-wavelength nanosecond pulse generation. These operation regimes are all realized with the same oscillator in the L-band. Compared with L-band mode-locked fiber lasers using CNTs or graphene as the mode lockers [30,31], pulses with shorter pulse duration can be generated in the single-soliton operation regime. The other two operation regimes are demonstrated for the first time in a GO mode-locked fiber laser oscillator.

2. EXPERIMENTAL DETAILS

The fabrication process of the GOSA is similar to that in [20]. For a clear demonstration of the detailed particulars of the GOSA sample utilized here, a brief description is also presented below. Firstly, some chemically oxidized graphite was ultrasonically agitated for preparing GO sheets with 1–3 atomic layers and diameter of 0.1–5 μm. The prepared ~0.6 mg GO sheets were poured into ~10 ml 0.1% sodium dodecyl sulfate (acting as a surfactant) aqueous solution, following by ~10 h ultrasonic agitation for adequately dispersing the GO sheets and then centrifugation for sedimentation of large GO clusters. Following this, the upper portion of the centrifuged solution was decanted and diluted in another container; by mixing with ~0.3 g polyvinylalcohol (PVA) powder and ultrasonic agitating for ~3 h at ~90°C, a uniform GO/PVA solution can be finally obtained. The last procedure was vertical oven evaporation of the GO/PVA solution for one or two days depending on the oven temperatures. This fabrication process is termed as the vertical evaporation method because the available GO/PVA film is formed mainly on the vertical wall of the polystyrene cell, not on the bottom. A GO/PVA composite sample prepared by this process is shown in Fig. 1(a). It can be clearly seen that both the GO concentration

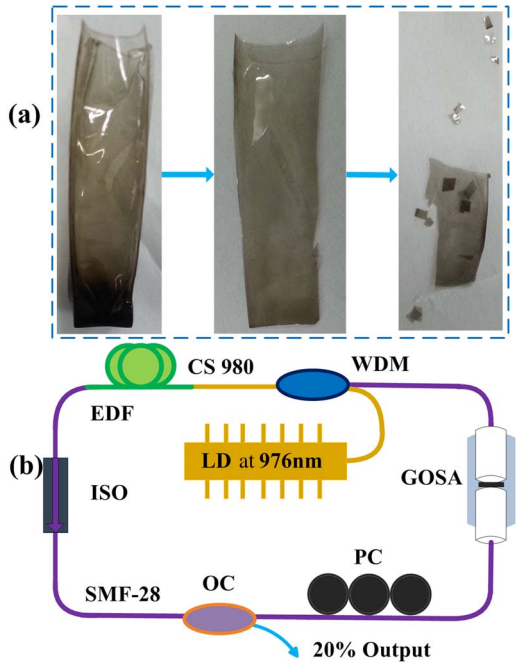

Fig. 1. (a) GOSA sample and its cutting process. (b) Schematic of the GO mode-locked fiber laser. WDM, wavelength division multiplexer; CS980 and SMF-28, two types of single-mode fibers from Corning Inc.; EDF, erbium-doped fiber; ISO, isolator; OC, output coupler; PC, polarization controller; GOSA, GO-based SA.

and film thickness continuously increase from the top to the bottom due to the incremental evaporation times experienced. The thickness information can be further measured by using a commercial digital micrometer. In detail, the GO/PVA composite exhibits optional thicknesses from 20 to 120 μm; thus, we can obtain the desired film pieces with different thicknesses simply by cutting it at different locations. Figure 1(a) shows the cutting process of the GO/PVA composite sample for obtaining the desired GOSA pieces. By choosing a suitable film piece with ~1 mm^2 area and ~60 μm thickness and sandwiching it between two fiber connectors, an integrated component to be used as an GOSA mode-locker can be assembled, which can be easily incorporated into a fiber ring cavity by fused splicing with other fiber segments.

The configuration of the fiber laser is schematically shown in Fig. 1(b). The gain medium is an 1.75 m Liekki Er110-4/125 EDF forward pumped by a 976 nm laser diode (LD) via a 980/1550 fused wavelength division multiplexer (WDM) coupler. Compared to typical EDF lasers, the EDF used here is exceptionally long considering its ultrahigh erbium doping concentration (in [18], the same kind of EDF was used but was only 30 cm in length), which is designed for operation at the L-band. Following the EDF, a polarization-independent isolator (ISO) and a polarization controller (PC) are used to ensure the unidirectional operation and adjust the polarization state, respectively. The PC has three paddles containing three spools of SMF-28 fiber. The laser output is directed by the 20% port of a 20/80 fused fiber optical coupler (OC). These devices, including the GOSA assembly, are connected by several segments of single-mode fibers, including ~10 cm CS-980 and several segments of SMF-28. The total length of the fiber ring cavity is ~8.5 m. For monitoring the output, several measurement equipments are used, including a photodiode power meter (Coherent Inc.), an optical spectrum analyzer (OSA, AQ6370B), an 1 GHz digital phosphor oscilloscope (Tekronix DPO7104C) coupled with a photodetector (Newport 818-BB-31), a real-time spectrum analyzer (for RF spectrum measurement), and an autocorrelator (FR-103 MN).

3. EXPERIMENTAL RESULTS AND DISCUSSIONS

Some chemical characteristics of the GOSA can be found in [20] measured by the second author, Yonggang Wang, such as the Raman spectrum (see Fig. 3 in [20]). One possible difference is the saturable absorption characteristics since different thickness might be employed. For self-starting of the passive mode-locking, the saturable absorption characteristics of the GOSA device are the most important factor. The saturable absorption property, that is, the power-dependent absorption, of the utilized GOSA is measured as follows. Here, the GOSA piece inserted in the fiber ring cavity exhibits thickness of ~60 μm, and its intensity-dependent measurement is shown in Fig. 2. The measurement is carried out by using a homemade seed laser with power amplification. The seed laser is a mode-locked EDF laser operating at 1596 nm, which can stably deliver ~770 fs pulses with ~21.79 MHz repetition rate [32]. The power amplification is performed by using a segment of EDF pumped with a 976 nm LD, as is schematically shown in Fig. 2(a). For obtaining continuously variable intensities, a variable optical attenuator (VOA) is used before the

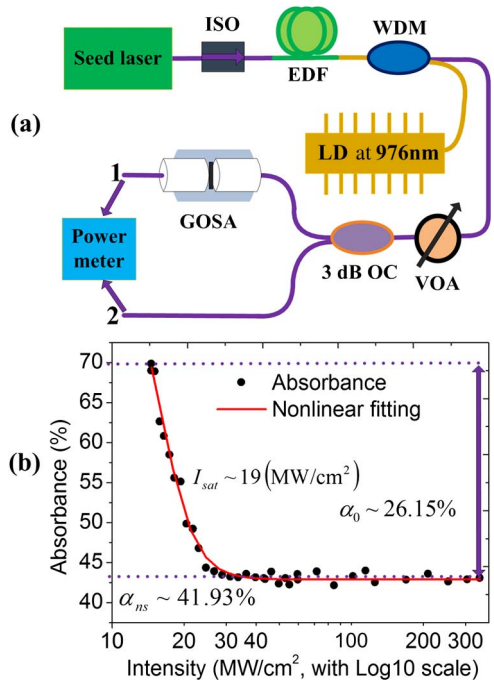

Fig. 2. (a) Measurement setup for the nonlinear absorbance characteristics of GOSA. VOA, variable optical attenuator. (b) Nonlinear absorbance of the utilized GOSA.

3 dB coupler. The nonlinear absorbance is determined by monitoring both the input and output average powers on the SA. For convenience and accuracy, the measurement system is in all-fiber format. As is shown in Fig. 2(b), the absorbance can be fitted with a two-level model. This model can be described by the following equation:

$$\alpha(I) = \alpha_0\left(1 + \frac{I}{I_{\text{sat}}}\right)^{-1} + \alpha_{\text{ns}}, \tag{1}$$

where I is the input laser intensity, I_{sat} is the saturation intensity (the intensity with the absorption coefficient of half the initial value [33]), $\alpha(I)$ is the intensity-dependent absorption coefficient, and α_0 and α_{ns} are the modulation depth and the nonsaturable loss, respectively. The results give a saturation intensity of ~19 MW/cm^2, modulation depth of ~26.15%, and nonsaturable loss of ~41.93%. For better demonstration of the nonlinear absorption characteristics, the horizontal coordinates are in Log10 scale. It can be seen that both the modulation depth and nonsaturable loss of the GOSA are larger than other similar reports [18,19,34], which is attributed to the fact that the thickness of our GOSA can be flexibly chosen. The long-time stability of such a GOSA is quite reliable, since no significant change of the saturable absorption characteristics can be observed even after exposure to air for more than 10 months. The GOSA's thermal stability is also experimentally examined. For hours of monitoring and times of tests, we have not observed any degradation of thermal stability when the film is inserted into the operating laser with pump powers of hundreds of milliwatts. Our times of experiments have demonstrated that the polymer-hosted film can function very well (including its long-time stability and repeatability) as an SA with low pump power (typically less than 500 mW) and low output power (such as several milliwatts). Thus, this type of SA can be a flexible and practical device for low-power

pulsed oscillator applications. Certainly, further optimizations might further improve its practicability such as introducing cooling devices, reducing the light-guiding losses, and so on. For higher power applications (watt-level), other host materials might be needed, such as hydrophilic quartz substrate, seen in [23].

Employing such a GOSA film piece in the laser resonator as demonstrated in Section 2, we can examine the mode-locked operation characteristics. Continuous wave (CW) operation starts when ~92.5 mW pump power is launched into the cavity. The mode-locking self-starts at ~108 mW pump power; the corresponding output average power is ~0.95 mW. Compared with typical C-band mode-locked EDF lasers [18,19], the threshold is higher, and the efficiency is lower, due to the lower gain in the L-band. According to the measurement of the utilized EDF, its gain at the lasing wavelength is only 21.75% of its typical value at 1530 nm (the gain at 1530 nm is ~100.9 dB/m, and the corresponding absorption is ~110.2 dB/m). However, compared with previous reports, these results are acceptable. In [30], the output power of L-band soliton lasing was only 0.711 mW at 123 mW pump power; it reached 1.18 mW when the pump power was 132 mW. The authors also attributed the low output power to the much lower gain of EDF at the L band. Although the authors in [31] presented a much lower mode-locking threshold and much higher output powers with the single-soliton regime, they had not presented the detailed gain value of the utilized EDF at the L-band, as well as the absorption and loss of the SA. Thus, we cannot know what contributes to the higher efficiency of their laser resonator.

Figure 3(a) shows a typical autocorrelation (AC) trace with Sech^2 (green solid line) fit giving a full width at half-maximum (FWHM) of ~657 fs. Considering the deconvolution factor for the Sech^2 profile, namely ~0.648, the pulse width should be ~426 fs. Figure 3(b) shows a typical output

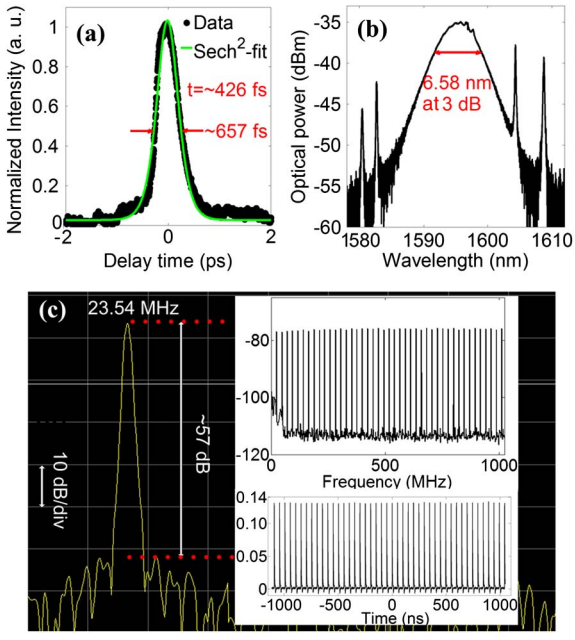

Fig. 3. Output characteristics from the stably mode-locked fiber laser. (a) AC trace, with $\mathrm{sec\,h}^2$ fitting. (b) Typical output spectrum with 3 dB bandwidth of ~6.58 nm. (c) RF spectrum around the fundamental repetition rate. Inset: RF spectrum with 1 GHz span.

spectrum, with central wavelength of ~1595.84 nm. The FWHM bandwidth, that is, the 3 dB bandwidth, is ~6.58 nm. The pulse duration is shorter and the bandwidth is wider than that reported in [30], where an L-band ultrafast fiber laser mode-locked by CNTs is demonstrated. The time bandwidth product (TBP) is calculated to be ~0.33. There is a minor deviation between the measured TBP value and the expected value of 0.315 for a transform-limited $\mathrm{sec\,h}^2$ pulse. The average intracavity group velocity dispersion (GVD) at the operation wavelength is estimated to be ~ – 19.2 ps^2/km, making the output pulses negatively chirped. The GVD-induced pulse chirping is the main reason for the TBP value slightly deviating from 0.315. Moreover, such a cavity design with net anomalous dispersion also favors soliton-like mode-locking. Another case that confirms the soliton-like operation is the appearance of two pairs of spectral sidebands (typically called Kelly sidebands), resulting from resonantly enhanced dispersive waves [35]. The four sidebands are at 1580.43, 1582.66, 1604.30, and 1608.76 nm, respectively.

Figure 3(c) presents a typical RF spectrum around the fundamental repetition rate of ~23.54 MHz, giving a signal-to-noise ratio (SNR) of ~57 dB. For further confirming the stability of the soliton operation regime, we also plot a RF spectrum up to 1 GHz, as seen in the upper right inset of Fig. 3(c). The uniformly distributed RF spectrum indicates that the soliton operation regime is well stable. Considering the fundamental repetition rate of ~23.54 MHz and the average output power of ~0.95 mW, the single pulse energy is ~40.36 pJ, a typical value of pulse energy directly output from an all-fiber laser oscillator operating at the soliton regime.

Although the operation of such a soliton regime is quite stable, the asymmetry profile and intensive pedestal of the recorded AC trace and the unsmooth spectral peak of the output spectrum indicate that some CW noises are circulated in the ring resonator along with intracavity soliton. The CW noises are formed due to modulation instability during the formation of the soliton. However, despite the CW noises, the pulse trains delivering from the resonator are clean, uniform, and stable, as can be seen in the lower right inset of Fig. 3(c).

Although the single soliton emission is well stable when the launched pump power is within the range from ~108 to ~122 mW, we can also obtain bound-state soliton operation through careful adjustments of the PC and changing the pump power. A typical result is shown in Fig. 4, which is achieved by carefully adjusting the PC and with ~141 mW pump power [36,37].

The output spectrum shown in Fig. 4(a) exhibits strong spectral modulation, which is caused by two closely bounded solitons [37]. The spectral modulation period is ~4.47 nm, corresponding to a Fourier-transformation soliton separation of ~1.9 ps in the time domain. Several sharp peaks can be seen on the spectrum, which is also caused by CW noise. The inset of Fig. 4(a) is an AC trace, which shows that two solitons are bounded together with partial intensity overlapping, agreeable with the spectral modulation period via the following relation:

$$\Delta\tau = \lambda^2/(c\Delta\lambda), \tag{2}$$

where $\Delta\tau$ is the pulse separation, λ is the central wavelength, c is the light velocity in vacuum, and $\Delta\lambda$ is the spectral modulation period. The separation is more than two times longer

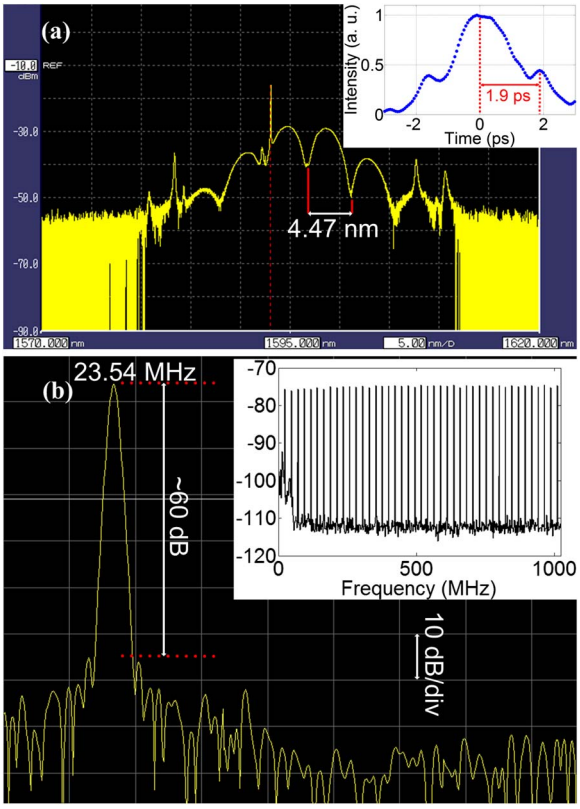

Fig. 4. (a) Output spectrum with the dual bound-state soliton operation; Inset: AC trace of the dual bound-state soliton. (b) RF spectrum around the fundamental repetition rate. Inset: RF spectrum with 1 GHz span.

than the FWHM of the previous single soliton; however, only when the FWHM of each soliton is longer than 1 ps could the soliton interaction be strong enough to form the bound state. These two inconsistent results indicate that the each bounded soliton here is longer than that with the single-soliton operation regime due to the power enhancement and PC adjustment. The pulse width variations induced by PC adjustment is a well-known phenomenon, and much early observation can be found in [38], where pulse width varying from less than 300 fs up to 500 fs can be achieved through adjustment of the PC. The recorded RF spectrum around the fundamental repetition rate is presented in Fig. 4(b), giving a SNR of ~60 dB, which is higher than the previous soliton operation regime, mainly due to higher output power (~1.78 mW) and intensity-overlap of two bounded solitons. The inset of Fig. 4(b) plots a RF spectrum up to 1 GHz with uniform distribution, which confirms the stability of the bound-state soliton operation.

The mechanism of the formation of the bound soliton can be analyzed as follows. According to our observations, the formation of the bound soliton is related to the launched pump power and the PC orientation. The enhancement of launched pump power can make more soliton formation and interaction. The influence of PC orientation is due to the linear cavity phase delay bias (LCPDB), and the shift of LCPDB can induce the relative phase change of the bounded solitons. With appropriate pump powers and polarization states, strong soliton interaction can be formed, that is, bound-state soliton formation.

Dual-frequency pulses in fiber lasers have been theoretically analyzed in [39], where the authors predicted that a dual-frequency pulse propagating in a fiber laser as a unit was possible. Here, we first experimentally demonstrate the generation of dual-wavelength pulses in a GO mode-locked fiber laser. In our cases, the operation regime with dual-wavelength pulse output is obtained with much higher pump power compared with the two operation regimes demonstrated previously. Figure 5 shows the output characteristics at ~446 mW launched pump power. With so high a pump power, the operation regime is mainly determined by the pump level; no influence of intracavity polarization state on the pulse behavior can be observed. Figure 5(a) shows the output spectrum, in which two main peak wavelengths can be seen: one centering at ~1572.93 nm, the other one centering at ~1588.37 nm, with ~15.44 nm separation. From Fig. 5(b) it can be clearly seen that the output is a single pulse; that is, the repetition period is approximately determined by the cavity length of ~8.5 m. Considering the output average power of ~15.2 mW, the pulse energy is ~0.65 nJ, much larger

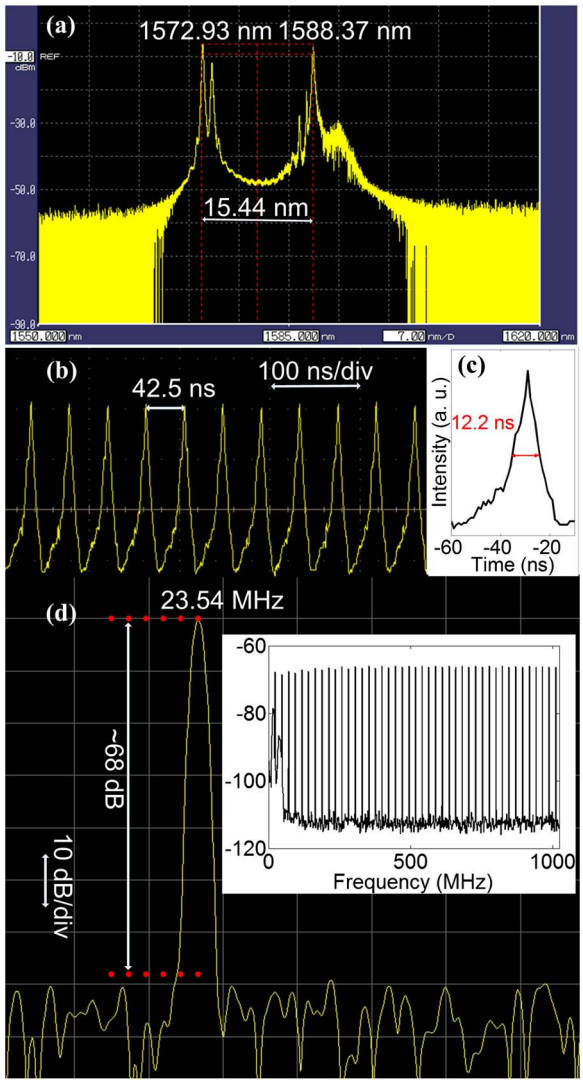

Fig. 5. Typical output at ~446 mW pump power. (a) Output spectrum. (b) Typical output pulse train. (c) Single pulse. (d) RF spectrum around the fundamental repetition rate. Inset: RF spectrum with 1 GHz span.

than that in the soliton operation regime. Figure 5(c) shows a plotted single-pulse envelope showing an asymmetry pulse profile with duration of ~12.2 ns in FWHM. Although the output pulse is much longer than that with the soliton regime, this operation regime is still mode-locking rather than *Q*-switching, for which one evidence is the cavity-length-determined repetition period. The single-pulse operation and operation stability can be further confirmed by the RF spectrum measurement as is shown in Fig. 5(d). A much higher SNR of ~68 dB can be achieved as shown, attributed to much higher output power and larger pulse energy. The large range distribution of the RF spectrum is also uniform as is plotted in the inset of Fig. 5(d).

Although the output spectrum of the dual-wavelength pulsed operation regime shows some likeness with the noise-like regime reported in [40], its formation might due to different mechanisms. Two characteristics of this regime that are much different from what demonstrated in [40] should be noticed. First, it is polarization independent; no matter how the PC is set, no significant change is observed both on the output spectrum and on the pulse train (or a single pulse). Our recorded spectrum and pulses are both stable with time as observed with a high-precision OSA (down to 0.02 nm) and high-speed oscilloscope respectively (up to 20 GS/s), not just an average effect. The single-pulse emission and its stability can also be confirmed by the RF spectra, as is shown in Fig. 5(d).

Another feature is that the dual-wavelength pulsed regime is only determined by launched pump powers. When the pump power approached ~446 mW, some unstable multiple soliton generation abruptly changes into the presented nanosecond pulse emission. The shorter wavelength centering at ~1572.93 nm is also simultaneously lased. Even the longer wavelength centering at ~1588.37 nm is also shorter than the soliton operation regime. This indicates that high gain dominates the interactions, overwhelming the reabsorption, due to the high launched pump power.

Thus, the mechanism for the formation of the dual-wavelength pulsed regime is due to the balance (or competition) between gain and reabsorption. The saturated gain effect that can be observed from region 5 in Fig. 6 further proves the competition between gain and reabsorption. The two-wavelength lasing resulting from gain and reabsorption competition destroyed the multiple soliton generation. Due to the ultranarrow bandwidths (~0.17 nm at ~1572.93 nm; ~0.15 nm at ~1588.37 nm) at the two lasing wavelengths (compared with the spectra with soliton emission), the generated pulses are very wide, with nanosecond scale.

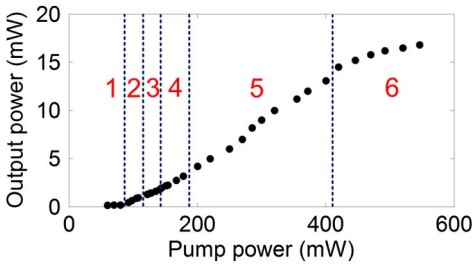

Fig. 6. Average output power with respect to the launched pump power with different regions: 1, no laser emission; 2, CW laser operation; 3, single-soliton operation; 4, bound-state soliton; 5, unstable multiple pulse generation; 6, dual-wavelength operation.

The evolution of average output power with respect to the launched pump powers with different regions is presented in Fig. 6. In region 1, no laser emission is observed, indicating that the launched pump power is almost absorbed, and the emission of fluorescence is quite weak. When the pump power is enhanced up to ~92.5 mW, CW laser starts, as seen in region 2. Regions 3 and 4 correspond to the single-soliton and bound-state soliton operations, respectively. In region 5 with pump power ranging from ~174 to ~420 mW, some unstable multiple pulses can be observed with a oscilloscope. Dual-wavelength operation can be achieved in region 6, and Fig. 5 is a typical case with ~446 mW pump power. No significant change can be seen from the evolution curve in the laser operation regions 2, 3, 4, and 5. However, when the laser starts the dual-wavelength operation the enhancement rate of the output power with respect to the pump power slows down, seen in region 6 in Fig. 6, which is due to the saturated gain effect around the lasing wavelengths.

4. CONCLUSIONS

We have successfully achieved three switchable mode-locking regimes in an EDF laser operating at the L-band by employing a GOSA device with optimized thickness. The obtained operation regimes include single-soliton operation with 426 fs pulse duration, bound-state soliton generation, and dual-wavelength nanosecond pulse generation. These results can find potential applications by employment of GOSA for achieving desired operation regimes.

ACKNOWLEDGMENTS

This research was supported by NSFC (61007054 & 61275144), the National High Technology Research and Development Program of China (2013AA031501&2012AA041203), the Improvement and Development Project of Shenzhen Key Lab (ZDSY20120612094924467), the Science and Technology Project of Shenzhen City (JCYJ20120613172042264, JCYJ20130329142040731), and Natural Science Foundation of SZU (No. 201221), and also supported by the Open Research Fund of the Key Laboratory of High Performance Complex Manufacturing, Central South University (No. HPCM-2013-10).

REFERENCES

1. A. Martinez and Z. Sun, "Nanotube and graphene saturable absorbers for fibre lasers," Nat. Photonics **7**, 842–845 (2013).
2. S. Y. Set, H. Yaguchi, Y. Tanaka, and M. Jablonski, "Laser mode locking using a saturable absorber incorporating carbon nanotubes," J. Lightwave Technol. **22**, 51–56 (2004).
3. S. Y. Set, H. Yaguchi, Y. Tanaka, and M. Jablonski, "Ultrafast fiber pulsed lasers incorporating carbon nanotubes," IEEE J. Sel. Top. Quantum Electron. **10**, 137–146 (2004).
4. D. Popa, Z. Sun, T. Hasan, W. B. Cho, F. Wang, F. Torrisi, and A. C. Ferrari, "74-fs nanotube-mode-locked fiber laser," Appl. Phys. Lett. **101**, 153107 (2012).
5. Z. Zhang, L. Wang, and Y. Wang, "Sub-100 fs and passive harmonic mode-locking of dispersion-managed dissipative fiber laser with carbon nanotubes," J. Lightwave Technol. **31**, 3719–3725 (2013).
6. Z. Yu, Y. Wang, X. Zhang, X. Dong, J. Tian, and Y. Song, "A 66 fs highly stable single wall carbon nanotube mode locked fiber laser," Laser Phys. **24**, 015105 (2014).
7. S. Yamashita, Y. Inoue, K. Hsu, T. Kotake, H. Yaguchi, D. Tanaka, M. Jablonski, and S. Y. Set, "5-GHz pulsed fiber Fabry–Pérot laser mode-locked using carbon nanotubes," IEEE Photon. Technol. Lett. **17**, 750–752 (2005).

8. K. Kieu and F. W. Wise, "All-fiber normal-dispersion femtosecond laser," Opt. Express **16**, 11453–11458 (2008).
9. M. Zhang, E. J. R. Kelleher, T. H. Runcorn, V. M. Mashinsky, O. I. Medvedkov, E. M. Dianov, D. Popa, S. Milana, T. Hasan, Z. Sun, F. Bonaccorso, Z. Jiang, E. Flahaut, B. H. Chapman, A. C. Ferrari, S. V. Popov, and J. R. Taylor, "Mid-infrared Raman-soliton continuum pumped by a nanotube-mode-locked sub-picosecond Tm-doped MOPFA," Opt. Express **21**, 23261–23271 (2013).
10. Q. Bao, H. Zhang, Y. Wang, Z. Ni, Y. Yan, Z. X. Shen, K. P. Loh, and D. Y. Tang, "Atomic-layer graphene as a saturable absorber for ultrafast pulsed laser," Adv. Funct. Mater. **19**, 3077–3083 (2009).
11. H. Zhang, D. Y. Tang, L. M. Zhao, Q. L. Bao, and K. P. Loh, "Large energy mode locking of an erbium-doped fiber laser with atomic layer graphene," Opt. Express **17**, 17630–17635 (2009).
12. Z. Sun, T. Hasan, F. Torrisi, D. Popa, G. Privitera, F. Wang, F. Bonaccorso, D. M. Basko, and A. C. Ferrari, "Graphene mode-locked ultrafast laser," ACS Nano **4**, 803–810 (2010).
13. D. Popa, Z. Sun, F. Torrisi, T. Hasan, F. Wang, and A. C. Ferraria, "Sub 200 fs pulse generation from a graphene mode-locked fiber laser," Appl. Phys. Lett. **97**, 203106 (2010).
14. A. Martinez and S. Yamashita, "10 GHz fundamental mode fiber laser using a graphene saturable absorber," Appl. Phys. Lett. **101**, 041118 (2012).
15. I. H. Baek, H. W. Lee, S. Bae, B. H. Hong, Y. H. Ahn, D. Yeom, and F. Rotermund, "Efficient mode-locking of sub-70-fs Ti:sapphire laser by graphene saturable absorber," Appl. Phys. Express **5**, 032701 (2012).
16. G. Zhu, X. Zhu, K. Balakrishnan, R. A. Norwood, and N. Peyghambarian, "Fe^{2+}:ZnSe and graphene *Q*-switched singly Ho^{3+}-doped ZBLAN fiber lasers at 3 μm," Opt. Mater. Express **3**, 1365–1377 (2013).
17. X. Zhao, Z. B. Liu, W. B. Yan, Y. Wu, X. L. Zhang, Y. Chen, and J. G. Tian, "Ultrafast carrier dynamics and saturable absorption of solution-processable few-layered graphene oxide," Appl. Phys. Lett. **98**, 121905 (2011).
18. G. Sobon, J. Sotor, J. Jagiello, R. Kozinski, M. Zdrojek, M. Holdynski, P. Paletko, J. Boguslawski, L. Lipinska, and K. M. Abramski, "Graphene oxide vs. reduced graphene oxide as saturable absorbers for Er-doped passively mode-locked fiber laser," Opt. Express **20**, 19463–19473 (2012).
19. J. Xu, J. Liu, S. Wu, Q. H. Yang, and P. Wang, "Graphene oxide mode-locked femtosecond erbium-doped fiber lasers," Opt. Express **20**, 15474–15480 (2012).
20. Y. G. Wang, H. R. Chen, X. M. Wen, W. F. Hsieh, and J. Tang, "A highly efficient graphene oxide absorber for *Q*-switched Nd:$GdVO_4$ lasers," Nanotechnology **22**, 455203 (2011).
21. Z. B. Liu, X. Y. He, and D. N. Wang, "Passively mode-locked fiber laser based on a hollow-core photonic crystal fiber filled with few-layered graphene oxide solution," Opt. Lett. **36**, 3024–3026 (2011).
22. X. Li, G. Q. Li, S. Z. Zhao, X. M. Wang, L. Yin, H. Huang, and X. M. Ma, "Diode-pumped Nd:YVO4 laser passively *Q*-switched with graphene oxide spin coated on ITO substrate," Laser Phys. **22**, 673–677 (2012).
23. Y. Wang, Z. Qu, J. Liu, and Y. H. Tsang, "Graphene oxide absorbers for watt-level high-power passive mode-locked Nd:$GdVO_4$ laser operating at 1 μm," J. Lightwave Technol. **30**, 3259–3262 (2012).
24. J. Liu, Y. G. Wang, Z. S. Qu, L. H. Zheng, L. B. Su, and J. Xu, "Graphene oxide absorber for 2 μm passive mode-locking Tm:$YAlO_3$ laser," Laser Phys. Lett. **9**, 15–19 (2012).
25. J. Xu, S. Wu, H. Li, J. Liu, R. Sun, F. Tan, Q. H. Yang, and P. Wang, "Dissipative soliton generation from a graphene oxide mode-locked Er-doped fiber laser," Opt. Express **20**, 23653–23658 (2012).
26. C. Liu, C. Ye, Z. Luo, H. Cheng, D. Wu, Y. Zheng, Z. Liu, and B. Qu, "High-energy passively *Q*-switched 2 μm Tm^{3+}-doped double-clad fiber laser using graphene-oxide-deposited fiber taper," Opt. Express **21**, 204–209 (2013).
27. M. Jung, J. Koo, P. Debnath, Y. W. Song, and J. H. Lee, "A mode-locked 1.91 μm fiber laser based on interaction between graphene oxide and evanescent field," Appl. Phys. Express **5**, 112702 (2012).
28. F. Bonaccorso, Z. Sun, T. Hasan, and A. C. Ferrari, "Graphene photonics and optoelectronics," Nat. Photonics **4**, 611–622 (2010).
29. O. Okhotnikov, A. Grudinin, and M. Pessa, "Ultra-fast fibre laser systems based on SESAM technology: new horizons and applications," New J. Phys. **6**, 177 (2004).
30. Z. Sun, A. G. Rozhin, F. Wang, V. Scardaci, W. I. Milne, I. H. White, F. Hennrich, and A. C. Ferrari, "L-band ultrafast fiber laser mode locked by carbon nanotubes," Appl. Phys. Lett. **93**, 061114 (2008).
31. J. Du, S. M. Zhang, H. F. Li, Y. C. Meng, X. L. Li, and Y. P. Hao, "L-band passively harmonic mode-locked fiber laser based on a graphene saturable absorber," Laser Phys. Lett. **9**, 896–900 (2012).
32. J. Q. Zhao, Y. G. Wang, P. G. Yan, S. C. Ruan, G. L. Zhang, H. Q. Li, and Y. H. Tsang, "An L-band graphene-oxide mode-locked fiber laser delivering bright and dark pulses," Laser Phys. **23**, 075105 (2013).
33. B. K. Garside and T. K. Lim, "Laser mode locking using saturable absorbers," J. Appl. Phys. **44**, 2335–2342 (1973).
34. G. Sobon, J. Sotor, and K. M. Abramski, "Passive harmonic mode-locking in Er-doped fiber laser based on graphene saturable absorber with repetition rates scalable to 2.22 GHz," Appl. Phys. Lett. **100**, 161109 (2012).
35. L. E. Nelson, D. J. Jones, K. Tamura, H. A. Haus, and E. P. Ippen, "Ultrashort-pulse fiber ring lasers," Appl. Phys. B **65**, 277–294 (1997).
36. D. Y. Tang, B. Zhao, L. M. Zhao, and H. Y. Tam, "Soliton interaction in a fiber ring laser," Phys. Rev. E **72**, 016616 (2005).
37. X. Wu, D. Y. Tang, X. N. Luan, and Q. Zhang, "Bound states of solitons in a fiber laser mode locked with carbon nanotube saturable absorber," Opt. Commun. **284**, 3615–3618 (2011).
38. M. L. Dennis and I. N. Duling, "Experimental study of sideband generation in femtosecond fiber lasers," IEEE J. Quantum Electron. **30**, 1469–1477 (1994).
39. J. M. Soto-Crespo, V. V. Afanasjev, N. N. Akhmediev, and G. E. Town, "Dual-frequency pulses in fiber lasers," Opt. Commun. **130**, 245–248 (1996).
40. S. Kobtsev, S. Kukarin, S. Smirnov, S. Turitsyn, and A. Latkin, "Generation of double-scale femto/pico-second optical lumps in mode-locked fiber lasers," Opt. Express **17**, 20707–20713 (2009).